Micrometre sized porous polymer beads as heterogeneous molecular catalysts

Michael B. Stammler, Anton Bauer, Mohammed H. Alkhurisi, Ferdinand Gigl, Florian M. Wisser

Angaben zur Veröffentlichung / Publication details:

Stammler, Michael B., Anton Bauer, Mohammed H. Alkhurisi, Ferdinand Gigl, and Florian M. Wisser. 2024. "Micrometre sized porous polymer beads as heterogeneous molecular catalysts." *Chemie Ingenieur Technik* 96 (3): 309–17. https://doi.org/10.1002/cite.202300023.

Micrometre-Sized Porous Polymer Beads as Heterogeneous Molecular Catalysts

Michael B. Stammler, Anton Bauer, Mohammed H. Alkhurisi, Ferdinand Gigl, and Florian M. Wisser*

DOI: 10.1002/cite.202300023

Supporting Information available online

Porous polymers have great potential as versatile, chemically stable catalyst supports. Yet, shaping of the resulting powders remains a challenge. Here, we demonstrate the use of suspension polymerisation to design micrometre-sized porous polymers beads containing metal binding sites. The good accessibility of the binding sites ensures high catalytic activity, which is demonstrated for two model reactions: photochemical CO_2 reduction and transfer hydrogenation of aromatic ketones. Importantly, the shaping of the host material does not affect the catalytic activity of the active site.

Keywords: Heterogeneous catalysis, Micrometre-sized beads, Porous organic polymer, Rhodium, Suspension polymerisation

Received: February 14, 2023; *revised:* April 04, 2023; *accepted:* May 08, 2023

1 Introduction

Microporous materials, including metal-organic frameworks (MOFs), covalent organic frameworks (COFs) and porous organic polymers (POPs) have gained enormous interest in the last decades for the heterogenization of molecular catalysts, including organometallic complexes and organo-catalysts [1–4]. Compared to the use of homogeneous catalysts, the use of heterogeneously supported catalysts in microporous solids simplifies separation and recyclability, particularly important for high-cost catalysts from the platinum metal group (PMG). More importantly, the support materials are more than an innocent host: They actually behave like ligands in molecular catalysis [5, 6].

Hence the catalytic activity of the active site can be controlled by design of the surrounding microporous materials [5, 6] and tailored for applications in various fields including photochemical CO_2 reduction and drug or fine chemical synthesis. Among MOFs, COFs and POPs, POPs stand out as the chemically most stable solids. However, as for MOFs and COFs, their typical syntheses yield almost exclusively fine powders with particle sizes well below 1 µm. Such powders are not suitable to allow for an easy implementation into industrial processes because of the difficult separation of solid and liquid phase or blockages induced by the powder. Overcoming this limitation remains one of the most important challenges for their implementation into large-scale processes [7].

One approach is the preparation of membranes or coatings. However, this would require very specific molecular architectures of both monomers and ligands for the catalyst, which strongly limits the choice of structures. An alternative is to shape the powdered materials into macroscopic bodies (few 100 µm to few mm) with sufficient mechanical and chemical stability, such as pellets, spheres or extrudates [8]. Extrusion and granulation processes are technically optimized for traditional catalytic materials, e.g., zeolites in batch or in continuous flow reactors [9]. However, these technologies cannot be directly transferred to POP materials. Suitable binders would need to be of polymeric nature, but adhesion between different polymers is typically low. Thus, high amounts of binder would be required, resulting in low loadings of active material [10–12].

[1,2]Michael B. Stammler, [1]Anton Bauer, [1]Mohammed H. Alkhurisi, [1]Ferdinand Gigl,
[1,3]Dr. Florian M. Wisser https://orcid.org/0000-0002-5925-895X (florian.wisser@fau.de)

[1]University of Regensburg, Institute of Inorganic Chemistry, Universitätsstraße 31, 93053 Regensburg, Germany.

[2]University of Augsburg, Institute of Physics, Chair of Solid State and Materials Science, Universitätsstraße 1, 86159 Augsburg, Germany.

[3]Erlangen Center for Interface Research and Catalysis, Friedrich-Alexander-Universität Erlangen-Nürnberg, Egerlandstraße 3, 91058 Erlangen, Germany.

This approach may also change the surface properties of the active material by forming a thin coating of binder on top of the surface of the porous material. Ultimately, this may result in a partial filling of the pore network itself, causing partial pore blocking [10].

In contrast, binder-free shaping of POPs would provide several advantages: The material would retain its intrinsic properties, including porosity and surface polarity. The accessibility and activity of the catalytic centres could likewise be retained. Additionally, a hierarchical pore structure can be established, ensuring efficient mass transport from larger transport pores [8], typically mesopores, into branching micropores in which the catalytic centres are situated.

Herein we demonstrate the use of micrometre-sized POP beads as porous macroligands for the heterogenization of molecularly defined catalysts. Spherical bipyridine containing porous organic polymers (Bpy-POP) were synthesized by suspension polymerisation of a mixture of 4,4′-divinyl-2,2′-bipyridine as binding site and both divinylbenzene and styrene, to adjust the site density of binding moieties in the final material. Pentamethylcyclopentadienylrhodium (Cp*Rh) tecton was infiltrated into the materials to yield the (bpy)Cp*Rh active site. The Rh-based catalysts were tested in two model reactions, the transfer hydrogenation of aryl ketones into the corresponding alcohols and the photochemical carbon dioxide reduction reaction.

2 Materials and Methods

2.1 Materials

Dibenzoyl peroxide (Luperox® A75, 75 %), divinylbenzene (80 %, main impurity vinyl-ethyl-benzene), Mowiol 40-88 (average M_w ~205 000 g mol^{-1}), nickel(II) chloride ethylene glycol dimethyl ether complex (98 %), 2-propanol (99.8 %), styrene (99 %) and *tris*(2,2′-bipyridyl)dichlororutheniu-m(II) hexahydrate were purchased from Sigma Aldrich. Acetonitrile (99.5 %) and silver nitrate (99.9 %) were purchased from Carl Roth, CO_2 (99.995 %) from Linde, 5,5′-divinyl-2,2′-bipyridine (97 %) from BLDpharm, pentamethylcyclopentadienylrhodium(III) chloride dimer ($[Cp^*RhCl_2]_2$, 97 %) from TCI, KOH (99.98 %) from Thermo Scientific and triethanolamine (99 %) from Acros Organics. Styrene and divinylbenzene were passed through a plug of basic Al_2O_3 prior to synthesis. All other chemicals were used as received without further purification.

2.2 General Methods

Nitrogen physisorption experiments at 77 K were carried out using a BELSORP-mini or BELSORP mini II. Prior to measurement the porous polymers were degassed at 80 °C under vacuum for at least 12 h. Apparent surface areas were estimated as single point BET areas at a partial pressure of 0.3 p/p_0.

IR spectra of fresh catalysts were recorded using a Varian 600-IR Series FT-IR spectrometer or a Thermo Scientific™ Nicolet™ iS™5 FT-IR spectrometer, as KBr pellets in transmission with a resolution of 1 cm^{-1} and 16 scans per sample.

Liquid NMR spectra were recorded on a Bruker AVANCE III HD 400 spectrometer (9.4 T, ^{1}H at 400.13 MHz, ^{13}C at 100.61 MHz). ^{1}H and ^{13}C spectra were referenced against the residual solvent signal. Quantitative NMR (*q*-NMR) spectra were recorded using a stem coaxial insert (Wilmad-LabGlass) filled with 0.25 M maleic acid in D_2O. Prior to measurement, the T_1 relaxation time was determined for all components in the reaction mixture and the recycle delay D1 was calculated for the signal with the longest T_1 according to D1 ≥ 5T_1. Also prior to measurement the filling ratio between the NMR tube and the inserts used was determined according to Henderson using maleic acid in D_2O and benzoic acid in DMSO-d_6 [13]. The quantitative uncertainty of the *q*-NMR spectroscopy was ≤ 2 %, which is considered to be sufficiently precise for *q*-NMR determination [14–16].

Scanning electron microscope (SEM) images were recorded on a Zeiss EVO MA15 scanning electron microscope using an acceleration voltage of 20 kV. Samples were coated with gold and palladium using a Quorum Technologies SC7620 Mini Sputter Coater. Energy-dispersive X-Ray (EDX) spectra were recorded using a Bruker Quantax EDS detector. For cross section analysis, POP beads were embedded in an epoxy resin matrix (Epo Fix Resin and EpoFix Hardener from Struers) and an appropriate amount was abrased mechanically to expose the centres of the beads.

A calibrated Leica DMRE optical microscope equipped with a Leica DFC 290 camera was used for optical measurements of bead sizes before and after exposure of the beads towards a given solvent (toluene, dioxane, tetrahydrofuran (THF), acetonitrile, 2-propanol).

Contents of carbon, hydrogen and nitrogen were determined using a Vario micro cube.

Inductively coupled plasma optical emission spectroscopy (ICP OES) analysis was done using an Activa from Jobin Yvon. Prior to ICP OES analysis, polymer beads were digested in a mixture of concentrated sulfuric and nitric acid at 300 °C in a Kjeldahl flask.

2.3 Synthesis

Bpy-POP: The synthesis was performed following a modified literature procedure [17]: For a typical synthesis, 50 mL of deionized water were deaerated in a 250 mL three-necked flask equipped with a mechanical stirrer and a reflux condenser, by bubbling a stream of argon through it for 30 min. After deaeration, the flask was kept under argon atmosphere and 125 mg polyvinyl alcohol (PVA, Mowiol® 40-88) were added under intense stirring. After the PVA was

completely dissolved, 2.5 mL toluene, 0.16 mL (1.40 mmol) styrene (ST), 2.0 mL (11.23 mmol) divinylbenzene (DVB), 603.0 mg (2.81 mmol) 5,5′-divinyl-2,2′-bipyridine and 45.4 mg (141 µmol) dibenzoyl peroxide were added. The solution was left to stir at room temperature for a few minutes and then heated to 70 °C for 20 h. After cooling down to room temperature, the polymer beads were isolated by centrifugation and washed several times with water. The beads were swollen in THF, after around 1 min ethanol was added and after another minute, they were isolated by centrifugation again. This process was repeated three times, then the beads were dried under vacuum at 80 °C over night.

CHN analysis [wt %] (calculated for 100 % conversion and dry material): C: 87.3 ± 0.1 (89.4), H: 7.0 ± 0.0 (7.4), N: 3.5 ± 0.1 (3.1).

DVB-POP: The synthesis was performed in the same way as for Bpy-POP beads, by replacing 5,5′-divinyl-2,2′-bipyridine with the equimolar amounts of DVB to reach the same degree of crosslinking. Instead of centrifugation, the polymer beads were filtrated between the washing steps.

CHN analysis [wt %] (calculated for 100 % conversion and dry material): C: 91.1 (92.1), H: 7.4 (7.9), N: 0.0 (0.0).

2.3.1 Metalation of Functionalised Polymer Beads

*Metalation with [RhCp*Cl]$^+$* [5]: A stock solution of [RhCp*Cl]NO_3 was prepared by adding 28.0 mg (44.9 µmol) [RhCp*Cl_2]$_2$ and 15.2 mg (89.4 µmol) $AgNO_3$ to a mixture of 5 mL acetonitrile and 1 mL MeOH. The yellow solution was stirred under light exclusion for 2 h, centrifuged to remove the white precipitate and then stored at 5 °C.

100 mg of Bpy-POP beads were suspended in 5 mL MeOH and 0.8 mL of the [RhCp*Cl]NO_3 stock solution were added. The mixture was stirred at 40 °C for 24 h and isolated by centrifugation, the intensely yellow polymer beads were washed with methanol four times and then dried under vacuum at room temperature.

CHN analysis [wt %] (calculated for 100 % conversion and dry material): C: 85.0 ± 0.1 (88.3), H: 7.0 ± 0.1 (7.4), N: 3.5 ± 0.1 (3.2)

ICP OES analysis detected 0.67 wt % Rh.

2.3.2 Photocatalytic Reduction of Carbon Dioxide

The catalysis was performed according to a modified literature procedure [5]. To a UV-VIS cuvette with a screw cap equipped with a rubber septum and a stirring bar (path length: 10 mm), Rh-functionalised Bpy-POP beads or [RhCp*(bpy)Cl_2] and 2 mL of a 1 mM solution of [Ru(bpy)$_3Cl_2$] (used as photosensitizer) in a mixture of acetonitrile and triethanolamine (5:1, V:V) were added. CO_2 was bubbled though the reaction mixture for 15 min, the cuvette was sealed and kept under CO_2 pressure during the reaction. The mixture was irradiated for 2 h using a sunlight simulator (MiniSol model LSH-7320, Newport, irradiance 1 sun at working distance). After irradiation, the solid was removed by centrifugation and the supernatant was analyzed by quantitative ^{1}H-NMR spectroscopy.

2.3.3 Rhodium-Catalyzed Transfer Hydrogenation of Aromatic Ketones

The catalysis was performed according to literature [6]. For a typical reaction, inside a glass vial Rh-functionalised Bpy-POP beads (equal to ~1 µmol Cp*Rh) were dispersed in approx. 2 mL of a degassed 0.011 mM solution of KOH in 2-propanol under argon atmosphere. The reaction mixture was stirred at 60 °C for 1 h, while the yellow polymer beads changed to a dark brown to black color. After 1 h, 0.166 mmol of the ketone were added and the mixture was stirred at 60 °C for 22 h. After cooling to room temperature, the reddish-brown beads were removed by centrifugation, washed with 2 mL diethyl ether and the resulting supernatant was added to the reaction solution. The organic phase was extracted with 1 mL brine, 1 mL deionized water and dried over $MgSO_4$. The conversion of aromatic ketones was analyzed by quantitative ^{1}H-NMR spectroscopy of the organic phase.

For recycling experiments, after extracting the catalyst with diethyl ether, the catalyst was washed with MeOH to remove inorganic impurities and dried at 60 °C under reduced pressure prior to use for the next catalytic cycle.

3 Results and Discussion

3.1 Synthesis and Material Characterization

Spherical POP beads were synthesised by suspension polymerisation modifying a literature procedure established for polystyrene beads with 2 % of divinylbenzene (DVB) as crosslinker [17]. To increase the mechanical stability and to control the swelling behaviour of the POP beads, we aimed to increase the amount of crosslinker up to 80 %. To introduce metal binding sites, commercially available 5,5′-divinyl-2,2′-bipyridine was used as a co-monomer together with a mixture of DVB and styrene (ST), the beads functionalised with bipyridine are labelled as Bpy-POP (Fig. 1). Both non-functionalised monomers (DVB, ST) are used to control the number of binding sites in the final material, DVB acts as additional cross-linker. For comparison, beads without bipyridine were synthesised, replacing 5,5′-divinyl-2,2′-bipyridine with the molar amount of DVB, the beads labelled DVB-POP. To also add a controlled amount of mesoporosity, toluene was added as a porogen to the monomer mixture (see below). To demonstrate the robustness of the synthesis procedure for the heterogenization of metal binding sites into POP-beads, also beads with phosphine moieties were successfully synthesised by replacing 5,5′-di-

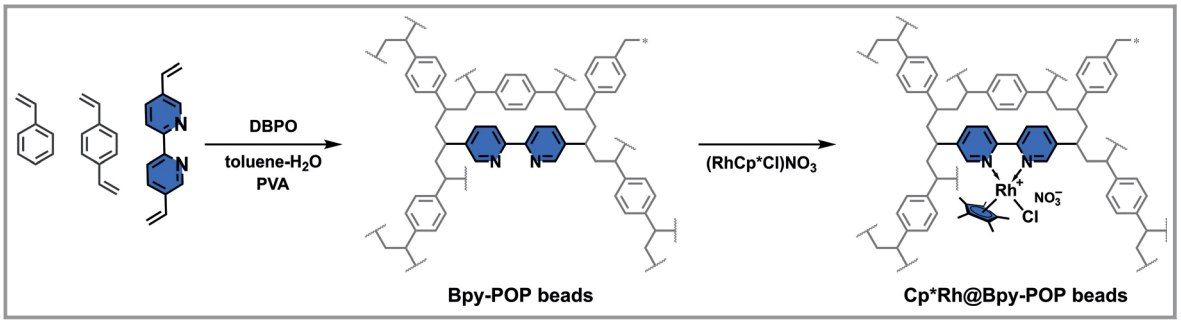

Figure 1. Radical suspension polymerisation-based synthesis routes for the micrometre-sized Bpy-POP beads and their subsequent functionalisation with the catalytically active pentamethylcyclopentadienylrhodium(III) (Cp*Rh) moiety to yield Cp*Rh@Bpy-POP catalyst.

vinyl-2,2′-bipyridine with diphenyl(4-vinylphenyl)phosphane, the beads labelled as Phos-POP (see Supporting Information Sect. 2).

As for other suspension polymerisations, the average particle size could be controlled by adjusting the stirring speed between 190 and 375 rpm. With increasing stirring speed, the average particle diameter, determined using SEM and optical microscopy, decreases from approx. 370 µm to 40 µm [17]. Of course, SEM and optical microscopy will provide information only of a small fraction of the batch. Thus, the average particle diameters were confirmed for a series of beads synthesised with different stirring speeds by sieve analysis of the entire batch. Sieve analysis confirms the representative nature of SEM and optical microscopy, the average particle size varies from 410 µm to 60 µm (Fig. 2).

The successful co-polymerisation was proven by IR spectroscopy as well as CHN analysis. In the IR spectra the integration of the bipyridine moiety is confirmed by the presence of bands which are attributed to the bipyridine in plane ring deformation at approx. 1540, 1250, 1130, 1020, 750 and 650 cm^{-1} as well as to the CH deformation vibration at 1465 cm^{-1} and ring-ring stretch vibrations at 1060 and 1025 cm^{-1} (Fig. 3a, 3b) [18]. Those bands are missing when the bipyridine moiety was replaced in the reaction mixture by additional DVB moieties. CHN analysis reveals a carbon to nitrogen ratio of 29.3 ± 0.3, in good agreement with the expected ratio of 32.1 for a complete co-polymerisation.

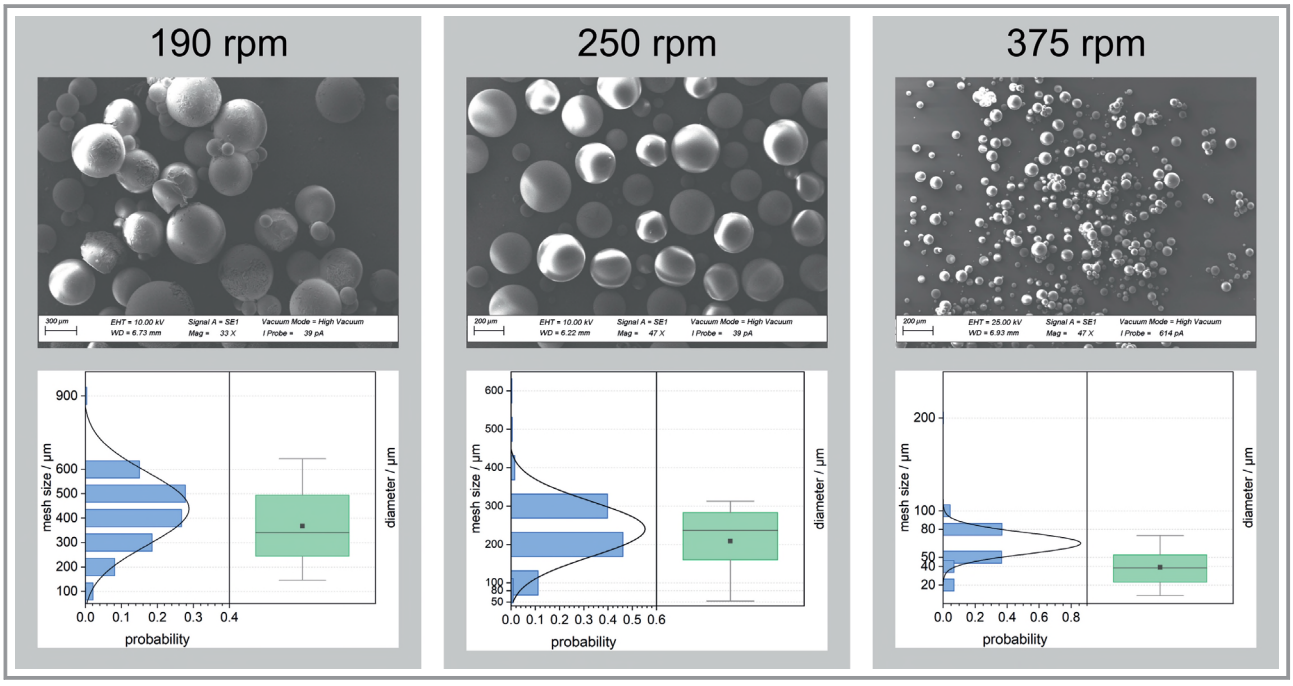

Figure 2. Comparison of SEM images and data yielded by gravimetric sieve analysis (left) and microscope analysis (right) for stirring speeds of 190 rpm, 250 rpm and 375 rpm. In the lower row, the left part shows the particle size distribution between the mesh size groups of the available sieves, fitted with a gaussian distribution function (black). On the right side, data from microscope analysis using ImageJ are represented in a box plot. The box diagram shows the upper and lower quartiles (box), the mean (square) and the median of the distribution (line) together with the 5th and 95th percentiles (whisker).

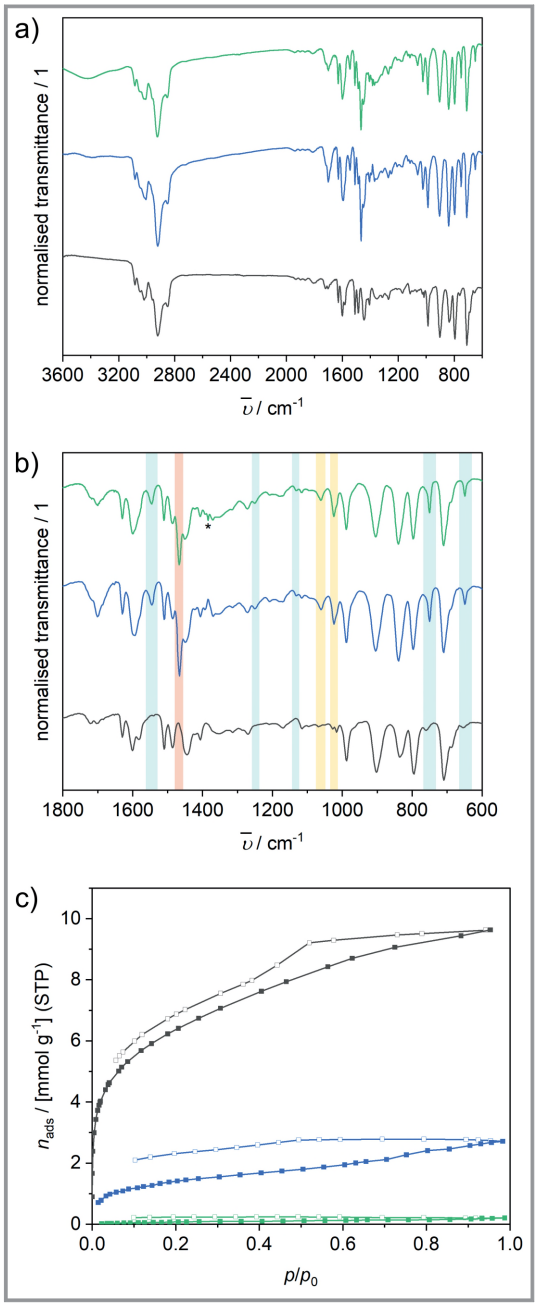

Figure 3. a) Complete IR spectra of spherical DVB-POP (grey), Bpy-POP (blue) and Cp*Rh@Bpy-POP beads (green). b) corresponding IR spectra in the fingerprint region. Characteristic bands of bipyridine plane ring deformation (light blue), CH deformation vibration (red) and ring-ring stretch vibrations (yellow) are highlighted. * labels nitrate stretching vibration. c) N_2 physisorption isotherms recorded at 77 K of spherical DVB-POP (grey), Bpy-POP (blue) and Cp*Rh@Bpy-POP beads (green).

N_2 physisorption isotherms were recorded to obtain some insights into the pore network of the different POP beads (Fig. 3c). The isotherms can be classified as a type I/type IV isotherm [19], with a pronounced hysteresis over the whole p/p_0 range. Such hysteresis between the adsorption and desorption branch of the material may be understood as a flexibility of the material even at 77 K. We however estimated the apparent surface area from N_2 physisorption experiments to be up to 500 m^2g^{-1} for DVB-POP and 100 m^2g^{-1} for Bpy-POP. Likewise, a surface of approx. 180 m^2g^{-1} was observed for Phos-POP. The decrease in apparent surface area after functionalisation with polar groups such as bipyridine moieties has also been observed in other porous polymers [20]. It may be explained by a non-favourable interaction of N_2 and the bipyridine-containing surface, different orientations of the quadrupolar N_2 on the surface depending on the composition (phenyl or biphenyl) [19], or a denser state after activation and cooling to 77 K of the beads containing the longer and thus more flexible bipyridine tecton [21]. The presence of mesopores is indicated by the continuous uptake of N_2 between 0.2 and 0.9 p/p_0 as well as the partial closing of the hysteresis at 0.5 p/p_0.

The solvent accessibility of Bpy-POP beads was demonstrated using swelling experiments. Under an optical microscope, the dry Bpy-POP beads were exposed to a variety of solvents, e.g., toluene, dioxane, THF, 2-Propanol and acetonitrile. Upon exposure to the solvent, a fast swelling was observed, reaching the final swollen state within a few seconds. The beads showed significant swelling and volume increase when exposed to those organic solvents. As expected, non-polar solvents led to higher volume increase (toluene up to 80 %) than polar aprotic or even polar protic solvents (2-propanol, acetonitrile: approx. 30 %). The swelling is reversed when the solvent dries out but can be repeated several times. Compared to the kinetics observed for the swelling of resin beads reported by Goworek and co-workers [22], we observed a much faster swelling, however, the maximal volume increase was lower. This can be explained by the much higher degree of crosslinking of the beads used in the scope of this work, giving the individual polymer strands a smaller margin for movement. Nevertheless, the fast swelling indicates exceptional accessibility of the polymer by the solvents [22]. This might hint towards a hierarchical porosity, where small micropores are connected to larger, open meso- and macropores, facilitating very fast diffusion.

3.2 Catalyst Design

For the design of catalytically active beads, the Bpy-POP beads were infiltrated with a methanolic solution of $[RhCp^*Cl]NO_3$ to create the catalytically active $[(bpy)RhCp^*Cl]NO_3$ sites. A Rh loading of 0.7 wt %, as determined by ICP OES, corresponding to a 5 % functionalisation of the available bipyridine binding sites was achieved. To evaluate the metal distribution, EDX mapping and line analysis over the cross section of RhCp*-loaded POP beads were performed. A radial distribution of the Rh is observed, resulting in a Rh-rich shell of approx. 5–10 µm

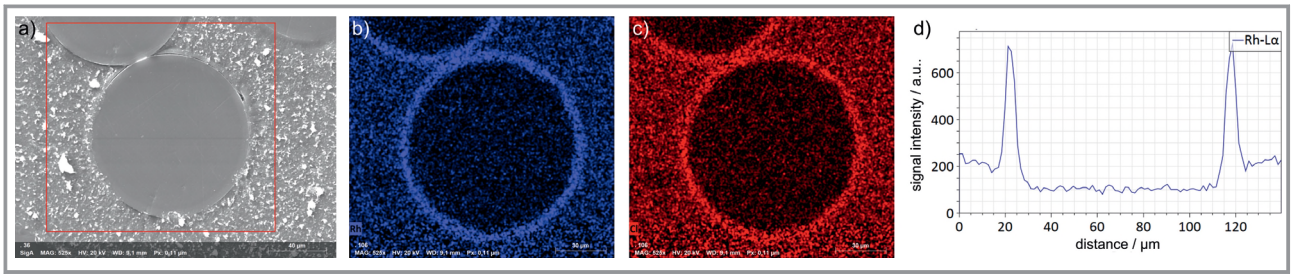

Figure 4. SEM image of a cross-section of a pristine Cp*Rh@Bpy-POP bead, together with EDX mapping of Rh (blue), Cl (red) and Rh signal intensity across the cross section. An overview of several beads is provided in the Supporting Information Fig. S1.

and a Rh-deficient core (Fig. 4). Assuming homogeneous nitrogen distribution over the cross section of the bead, such a core-shell structure is expected from the Rh to bipyridine ratio of 1 to 20 and the high affinity of the RhCp* moiety to the bipyridine moiety. The volume ratio between the Rh-rich shell and the Rh-deficient core can be estimated to be around 0.1. Note that a similar behaviour was observed when the Bpy-POP beads were infiltrated with a $NiCl_2$ precursor solution (see SI Sect. 3 for further discussion).

As for other Cp*Rh-loaded microporous materials, no significant change in the IR spectrum before and after metalation can be detected, except for the presence of the characteristic nitrate vibration at approx. 1380 cm^{-1} (Fig. 3b) [23, 24]. Also, in line with literature reports [5, 25–28], the apparent surface area as deduced from N_2 physisorption isotherms at 77 K is strongly reduced (Fig. 3c), which however is not crucial for application in liquid phase catalysis (see below).

3.3 Catalytic Application

The accessibility and catalytic activity of the RhCp* active sites within the POP-beads were first demonstrated in photocatalytic reduction of CO_2 (Fig. 5). The reaction was performed in a CO_2-saturated 1 mM $Ru(bpy)_3Cl_2$ solution of acetonitrile and triethanolamine under visible light irradiation. In the photocatalytic cycle $Ru(bpy)_3Cl_2$ is required as light harvesting moiety, while triethanolamine is supposed to act as electron and proton donor [29, 30]. Although the use of such large particles may lead to significant light scattering and thus loss of incoming photons, a turnover frequency (*TOF*) of up to 14 h^{-1} was achieved. The activity is comparable to the activity of other Cp*Rh@POP catalysts [5], and higher than the activity of the same active site heterogenized in MOFs (Fig. 5) [5, 31–33]. No formic acid production was observed in the absence of $Ru(bpy)_3Cl_2$ or under exclusion of light, confirming the photocatalytic nature of the reaction. Also, in the absence of CO_2, no formic acid was produced, confirming that formic acid originates form CO_2 and neither from decomposition of the framework nor of the solvent.

As a second application, the beads were investigated in the transfer hydrogenation of aromatic ketones into the corresponding alcohols. For comparison with reported activities in the literature, the catalytic activity was studied in isopropanol, serving both as solvent and hydrogen donor, at 60 °C under an Ar atmosphere [6]. Using acetophenone as substrate, a turnover number (*TON*) of 31 was observed after 22 h. A lower activity has been reported for the same active site heterogenized within a purely microporous, powdered POP (Fig. 6) [6]. Replacing acetophenone with 4-chloroacetophenone gave similar *TON* of approx. 33. For cyclic ketones such as α-tetralone the *TON* decreases to approx. 13, while ketones with longer alkyl chains or bulkier aromatic moieties yields increased catalytic activities around 40.

In particular the result for the sterically more demanding propiophenone is remarkable and demonstrates the benefit of having additional mesopores inside the framework compared to purely microporous materials. In the latter case, a decrease in catalytic activity by a factor 4 has been observed

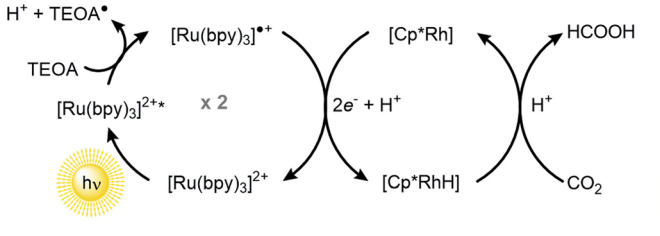

macroligand of [Cp*Rh]	TOF / h^{-1}	Ref
Bpy-POP beads	14	this work
BpyMP-1	2 – 28 [a]	5
MOF-253	4	5
UiO-67	1.3 – 7.5	5, 31, 33
PW_{12}@UiO-67	2.4	33
MIL-101	0.66	32

Figure 5. Left: Schematic representation of the photocatalytic cycle involved in the reduction of CO_2 to formic acid, according to literature [29, 30]. Right: Comparison of catalytic activity of Cp*Rh@ Bpy-POP beads to other microporous macroligands containing the same active site. a) Different functionalisation of the bipyridine moiety.

by some of the authors when replacing acetophenone with propiophenone [6], under otherwise identical conditions,

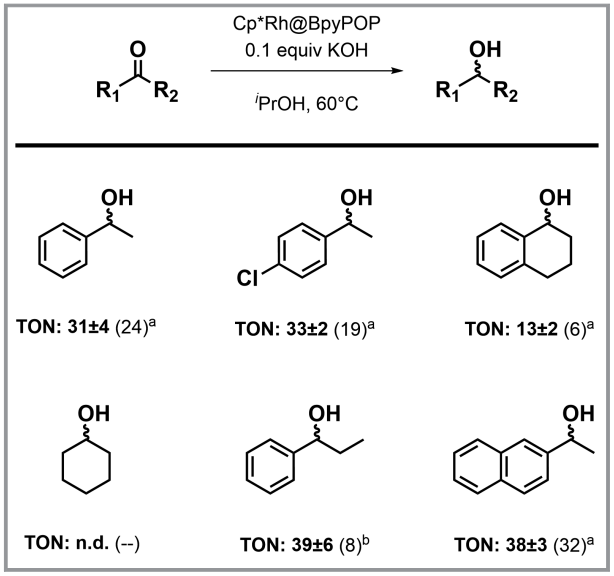

Figure 6. Scope of the reduction of various ketones. Reaction conditions: Ketone : KOH : Cp*Rh@POP = 160:16:1, 60 °C in *iso*-propanol. *TON* values in brackets are from reference [6] using the amine functionalised catalyst Cp*Rh@BpyMP-1-NH_2 under otherwise identical conditions. a) *TON* after 24 h, b) *TON* after 48 h; n.d.: not determined.

while for the mesoporous POP beads the activity was even slightly increased (Fig. 6).

The recyclability of the catalyst was demonstrated by simple centrifugation, washing with MeOH, and drying under reduced pressure at 60 °C. Spent catalysts showed unaltered catalytic activity with a *TON* of 33 ± 5. The recycling experiments were conducted at ca. 20 % conversion of acetophenone. Thus, the reaction is not limited by the availability of the substrate [34]. IR spectroscopic (Fig. S2) and SEM-EDX investigations do not indicate any decomposition or degradation of the catalysts. EDX mapping highlights a core-shell structure of the Rh distribution also for the spent catalyst. Again, the Rh-rich shell is about 5–10 µm wide, confirming an unchanged radial rhodium distribution (Fig. 7).

4 Conclusion

In this study we designed micrometre-sized porous polymer beads as porous macroligands for the heterogenization of molecular Rh complexes. The solvent accessibility and swelling behaviour of the polymer beads were demonstrated using optical microscopy for a series of organic solvents. The beads are best accessible for nonpolar solvents followed by polar aprotic and polar protic solvents, with a volume increase of at least 30 %. The good accessibility of the binding sites ensures controllable functionalisation with, e.g., RhCp* moieties as catalytically active metal centres, and their accessibility for catalytic reactions. The catalytic potential of the Rh-functionalised beads has been demonstrated for two model reactions: photochemical CO_2 reduction and transfer hydrogenation of aromatic ketones. Importantly, the shaping of the host material does not affect the catalytic activity of the active site. Moreover, the introduction of mesopores leads to a higher conversion of sterically demanding ketones, as compared to purely microporous materials. Having demonstrated the potential of micrometre-sized porous polymer beads as porous solid macroligands, their easy and scalable synthesis allows for their gram-scale preparation, thus we expect to see the application of those POP materials in technically relevant continuous flow processes in the future.

Supporting Information

Supporting Information for this article can be found under DOI: https://doi.org/10.1002/cite.202300023. This section includes additional references to primary literature relevant for this research [35–38].

Acknowledgment

F. M. W. gratefully acknowledges financial support from the DECHEMA e. V. (Max-Buchner-Forschungsstipendium #3815). The authors thank Dr. Jérôme Canivet for providing access to N_2 physisorption measurements and ICP OES analysis, Chantal Lorentz for recording ^{31}P solid state NMR

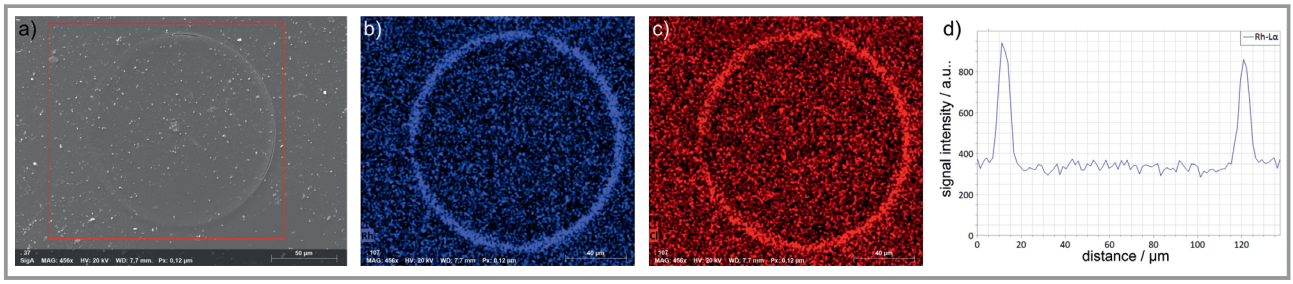

Figure 7. SEM image of a cross section of a spent Cp*Rh@Bpy-POP bead after transfer hydrogenation of acetophenone for 22 h at 60 °C, together with EDX mapping of Rh (blue), Cl (red) and Rh signal intensity over the cross section. An overview of several beads is provided in the Supporting Information Fig. S1.

spectra as well as Ulrike Schießl for SEM analysis. The authors gratefully acknowledge Prof. Baeumner for providing access to a calibrated light microscope. Open access funding enabled and organized by Projekt DEAL.

Symbols used

n_{ads}	[cm^3g^{-1}]	adsorbed amount
p/p_0	[–]	partial pressure
S_{BET}	[m^2g^{-1}]	apparent surface area
TOF	[h^{-1}]	turnover frequency
TON	[–]	turnover number
V	[L]	volume

Abbreviations

bpy	2,2′-bipyridine
BpyMP-1	bipyridine-containing microporous polymer
Bpy-POP	2,2′bipyridine-based porous organic polymer
COF	covalent organic framework
Cp*Rh	pentamethylcyclopentadienylrhodium(III)
DVB	divinylbenzene
DVB-POP	divinylbenzene-based porous organic polymer
EDX	energy dispersive X-ray
IR	infrared
ICP OES	inductively coupled plasma optical emission spectroscopy
MeOH	methanol
MOF	metal-organic framework
NMR	nuclear magnetic resonance
POP	porous organic polymer
PVA	polyvinyl alcohol
SEM	scanning electron microscope
ST	styrene
STP	standard temperature and pressure
THF	tetrahydrofuran

References

[1] M. Rose, R. Palkovits, in *Metal Organic Frameworks as Heterogeneous Catalysts* (Eds: F. X. Llabrés i Xamena, J. Gascon), Royal Society Of Chemistry, London **2013**.
[2] J.-S. M. Lee, A. I. Cooper, *Chem. Rev.* **2020**, *120 (4)*, 2171–2214. DOI: https://doi.org/10.1021/acs.chemrev.9b00399
[3] M. Viciano-Chumillas, M. Mon, J. Ferrando-Soria, A. Corma, A. Leyva-Pérez, D. Armentano, E. Pardo, *Acc. Chem. Res.* **2020**, *53 (2)*, 520–531. DOI: https://doi.org/10.1021/acs.accounts.9b00609
[4] C. Krishnaraj, H. S. Jena, K. Leus, P. Van Der Voort, *Green Chem.* **2020**, *22 (4)*, 1038–1071. DOI: https://doi.org/10.1039/C9GC03482J
[5] F. M. Wisser, P. Berruyer, L. Cardenas, Y. Mohr, E. A. Quadrelli, A. Lesage, D. Farrusseng, J. Canivet, *ACS Catal.* **2018**, *8 (3)*, 1653–1661. DOI: https://doi.org/10.1021/acscatal.7b03998
[6] F. M. Wisser, Y. Mohr, E. A. Quadrelli, D. Farrusseng, J. Canivet, *ChemCatChem* **2018**, *10 (8)*, 1778–1782. DOI: https://doi.org/10.1002/cctc.201701836
[7] Y. Tian, G. Zhu, *Chem. Rev.* **2020**, *120 (16)*, 8934–8986. DOI: https://doi.org/10.1021/acs.chemrev.9b00687
[8] W. Schwieger, A. G. Machoke, T. Weissenberger, A. Inayat, T. Selvam, M. Klumpp, A. Inayat, *Chem. Soc. Rev.* **2016**, *45 (12)*, 3353–3376. DOI: https://doi.org/10.1039/C5CS00599J
[9] F. Akhtar, L. Andersson, S. Ogunwumi, N. Hedin, L. Bergström, *J. Eur. Ceram. Soc.* **2014**, *34 (7)*, 1643–1666. DOI: https://doi.org/10.1016/j.jeurceramsoc.2014.01.008
[10] S. Hock, M. Rose, *Chem. Ing. Tech.* **2020**, *92 (5)*, 525–531. DOI: https://doi.org/10.1002/cite.201900149
[11] S. Periyasamy, M. Naushad, N. Viswanathan, *Environ. Sci. Water Res. Technol.* **2020**, *6 (3)*, 851–863. DOI: https://doi.org/10.1039/C9EW01096C
[12] A. V. Bavykina, E. Rozhko, M. G. Goesten, T. Wezendonk, B. Seoane, F. Kapteijn, M. Makkee, J. Gascon, *ChemCatChem* **2016**, *8 (13)*, 2217–2221. DOI: https://doi.org/10.1002/cctc.201600419
[13] T. J. Henderson, *Anal. Chem.* **2012**, *74 (1)*, 191–198. DOI: https://doi.org/10.1021/ac010809+
[14] S. K. Bharti, R. Roy, *TrAC Trends Anal. Chem.* **2012**, *35*, 5–26. DOI: https://doi.org/10.1016/j.trac.2012.02.007
[15] D. J. Boston, C. Xu, D. W. Armstrong, F. M. MacDonnell, *J. Am. Chem. Soc.* **2013**, *135 (44)*, 16252–16255. DOI: https://doi.org/10.1021/ja406074w
[16] A. Rosas-Hernández, H. Junge, M. Beller, *ChemCatChem* **2015**, *7 (20)*, 3316–3321. DOI: https://doi.org/10.1002/cctc.201500494
[17] N. M. Sekerak, K. M. Hutchins, B. Luo, J. G. Kang, P. V. Braun, Q. Chen, J. S. Moore, *Eur. Polym. J.* **2018**, *101 (January)*, 202–210. DOI: https://doi.org/10.1016/j.eurpolymj.2018.01.028
[18] E. Castellucci, L. Angeloni, N. Neto, G. Sbrana, *Chem. Phys.* **1979**, *43 (3)*, 365–373. DOI: https://doi.org/10.1016/0301-0104(79)85204-0
[19] M. Thommes, K. Kaneko, A. V. Neimark, J. P. Olivier, F. Rodriguez-Reinoso, J. Rouquerol, K. S. W. Sing, *Pure Appl. Chem.* **2015**, *87 (9–10)*, 1051–1069. DOI: https://doi.org/10.1515/pac-2014-1117
[20] M. Alves Fávaro et al., *ACS Appl. Mater. Interfaces.* **2022**, *14 (12)*, 14182–14192. DOI: https://doi.org/10.1021/acsami.1c24713
[21] E. Troschke, K. D. Nguyen, S. Paasch, J. Schmidt, G. Nickerl, I. Senkovska, E. Brunner, S. Kaskel, *Chem. – A Eur. J.* **2018**, *24 (70)*, 18629–18633. DOI: https://doi.org/10.1002/chem.201804373
[22] P. Krasucka, P. Mergo, G. Wójcik, J. Goworek, *Chem. Eng. Sci.* **2018**, *190*, 21–27. DOI: https://doi.org/10.1016/j.ces.2018.05.060
[23] T. P. Gerasimova, S. A. Katsyuba, *Dalt. Trans.* **2013**, *42 (5)*, 1787–1797. DOI: https://doi.org/10.1039/C2DT31922E
[24] J. Coates, in *Encyclopedia of Analytical Chemistry*, John Wiley & Sons, Hoboken, NJ **2006**.
[25] K. K. Tanabe et al., *Chem. Sci.* **2013**, *4 (6)*, 2483. DOI: https://doi.org/10.1039/c3sc22268c
[26] J.-X. Jiang, C. Wang, A. Laybourn, T. Hasell, R. Clowes, Y. Z. Khimyak, J. Xiao, S. J. Higgins, D. J. Adams, A. I. Cooper, *Angew. Chem., Int. Ed.* **2011**, *50 (5)*, 1072–1075. DOI: https://doi.org/10.1002/anie.201005864
[27] Y. Mohr et al., *ACS Catal.* **2021**, *11 (6)*, 3507–3515. DOI: https://doi.org/10.1021/acscatal.1c00209
[28] M. Henrion, Y. Mohr, K. Janssens, S. Smolders, A. L. Bugaev, O. A. Usoltsev, E. A. Quadrelli, F. M. Wisser, D. E. De Vos, J. Canivet, *ChemCatChem* **2022**, *14 (19)*, 9–25. DOI: https://doi.org/10.1002/cctc.202200649

[29] Y. Yamazaki, H. Takeda, O. Ishitani, *J. Photochem. Photobiol. C Photochem. Rev.* **2015**, *25 (4)*, 106–137. DOI: https://doi.org/10.1016/j.jphotochemrev.2015.09.001
[30] A. Solé-Daura, Y. Benseghir, M.-H. Ha-Thi, M. Fontecave, P. Mialane, A. Dolbecq, C. Mellot-Draznieks, *ACS Catal.* **2022**, *12 (15)*, 9244–9255. DOI: https://doi.org/10.1021/acscatal.2c02088
[31] M. B. Chambers et al., *ChemSusChem* **2015**, *8 (4)*, 603–608. DOI: https://doi.org/10.1002/cssc.201403345
[32] X. Wang, F. M. Wisser, J. Canivet, M. Fontecave, C. Mellot-Draznieks, *ChemSusChem* **2018**, *11 (18)*, 3315–3322. DOI: https://doi.org/10.1002/cssc.201801066
[33] Y. Benseghir et al., *J. Am. Chem. Soc.* **2020**, *142 (20)*, 9428–9438. DOI: https://doi.org/10.1021/jacs.0c02425
[34] U. I. Kramm, R. Marschall, M. Rose, *ChemCatChem* **2019**, *11 (11)*, 2563–2574. DOI: https://doi.org/10.1002/cctc.201900137
[35] D. Massiot, F. Fayon, M. Capron, I. King, S. Le Calvé, B. Alonso, J.-O. Durand, B. Bujoli, Z. Gan, G. Hoatson, *Magn. Reson. Chem.* **2002**, *40 (1)*, 70–76. DOI: https://doi.org/10.1002/mrc.984
[36] J. Bai, Y. Huang, Q. Gong, X. Liu, Y. Li, J. Gan, M. Zhao, Y. Shao, D. Zhuang, J. Liang, *Carbon* **2018**, *137*, 493–501. DOI: https://doi.org/10.1016/j.carbon.2018.05.058
[37] E. Schade, F. M. Wisser, M. Franke, A. Weiz, M. Werheid, J. R. Martin, S. Kaskel, J. Grothe, *ChemNanoMat* **2018**, *4 (9)*, 1000–1006. DOI: https://doi.org/10.1002/cnma.201800226
[38] M. L. Niven, G. C. Percy, *Transit. Met. Chem.* **1978**, *3 (1)*, 267–271. DOI: https://doi.org/10.1007/BF01393566

